Title
Three-body dissociation dynamics of the low-lying Rydberg states of H-3 and D-3

Journal
Physical Review Letters, 93(15)

ISSN
0031-9007

Authors
Laperle, C M
Mann, J E
Clements, T G
et al.

Publication Date
2004-10-01

Peer reviewed

Three-Body Dissociation Dynamics of the Low-Lying Rydberg States of H_3 and D_3

Christopher M. Laperle, Jennifer E. Mann, Todd G. Clements, and Robert E. Continetti*
Department of Chemistry and Biochemistry, University of California, San Diego, 9500 Gilman Drive, La Jolla, California 92093-0340, USA
(Received 19 April 2004; published 8 October 2004)

The dynamics of the three-body dissociative charge exchange of fast (12 keV) H_3^+ and D_3^+ with Cs have been studied using multiparticle translational spectroscopy. The observed partitioning of product momenta was found to be state-specific and yields insights into the nuclear motion during dissociation for the three lowest-lying $2s\ ^2A_1'$, $2p\ ^2A_2''$, and $3p\ ^2E'$ metastable Rydberg states of H_3 and the $2s\ ^2A_1'$ and $2p\ ^2A_2''$ states for D_3. These results provide direct empirical information on the nonadiabatic couplings that govern the three-body dissociation of the lowest-lying Rydberg states of H_3 and D_3.

DOI: 10.1103/PhysRevLett.93.153202 PACS numbers: 34.60.+z, 34.50.–s, 34.70.+e

H_3 is the simplest neutral triatomic molecule and serves as a prototypical system for experimental and theoretical studies. The metastable states of H_3, below the ionization threshold for the production of $H_3^+ + e^-$, consist of a manifold of Rydberg states that dissociate via nonadiabatic interactions with the unbound ground electronic state. Consequently, there are no states of neutral H_3 that live for longer than $\sim 1\ \mu$s [1,2]. H_3^+, however, is stable and initiates many chemical reactions that yield exotic chemical species in interstellar space [3]. Optical spectra of H_3^+, in conjunction with simple kinetic models, are used to understand the composition of the interstellar medium [4]. The models assume that an important destruction process for H_3^+ in diffuse clouds is dissociative recombination (DR) with free electrons [5]:

$$H_3^+ + e^- \rightarrow H_3^* \rightarrow \begin{matrix} H_2 + H \\ H + H + H \end{matrix}. \tag{1}$$

Experimental and theoretical determinations of the rate coefficient for this process k_{DR} have historically been at odds [6]. However, recent experiments on fast (MeV) ion beams in storage rings by Strasser *et al.* [7] and McCall *et al.* have determined a value for k_{DR} [8] that is generally consistent with the recent theoretical treatment of Kokoouline *et al.* [9,10]. A quantitative understanding of H_3, however, requires going beyond rate coefficients to gain insight into the energy and state dependence of the dissociation dynamics.

The equilibrium geometry of H_3^+ and the Rydberg states of H_3 is an equilateral triangle with D_{3h} electronic and C_{3v} nuclear symmetry. Figure 1 illustrates the nuclear configurations of these species and the three normal vibrational modes denoted Q_1, Q_x, and Q_y. An important contribution to the dissociative recombination of H_3^+ involves nonadiabatic transitions from high-lying Rydberg states to the lower-lying Rydberg states that are finally predissociated by the ground $2p\ ^2E'$ state [11]. The dissociative $2p\ ^2E'$ ground-state is doubly degenerate in D_{3h} symmetry and undergoes a Jahn-Teller distortion, lifting the degeneracy. This causes the ground-state potential energy surface (PES) to split into upper and lower repulsive sheets, corresponding to the three- and two-body dissociation limits respectively [12]. Nonadiabatic coupling of the metastable Rydberg states to the upper repulsive sheet governs the dynamics of three-body dissociation. Previously, measurements of three-body dynamics have been reported for high-lying Rydberg states [13] and for selected $n = 3$ Rydberg states [14–17]. In this Letter, we report the first direct measurement of the three-body dissociation dynamics of the two lowest $2s\ ^2A_1'$ and $2p\ ^2A_2''$ Rydberg states of H_3 and D_3. Additionally, we present data on the $3p\ ^2E'$ state of H_3 consistent with recent work [17] that uses a different method of preparation.

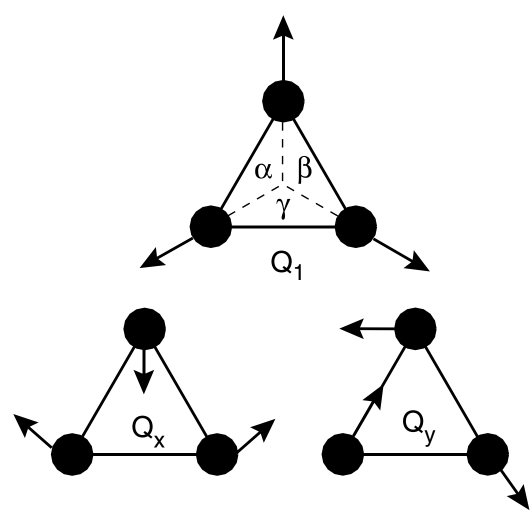

FIG. 1. The equilibrium nuclear configuration and distortions due to the normal vibrational modes of H_3: the symmetric mode Q_1 preserving C_{3v} symmetry and the degenerate modes Q_x and Q_y preserving C_{2v} and C_s symmetry, respectively. The angles between the c.m. momentum vectors (indicated by the dashed lines) of the atomic fragments are represented by α, β, and γ.

The Rydberg states of H_3 were produced by resonant and nonresonant charge exchange (CE) of a fast (12 keV) H_3^+ ion beam with Cs vapor:

$$H_3^+ + Cs \rightarrow H_3^* + Cs^+. \quad (2)$$

The states of H_3 formed are largely dependent on resonances due to the matching of ionization potentials of H_3^* and Cs; however, the cross section for nonresonant CE (NRCE) increases considerably with relative velocity [18]. Since the transitions occur on time scales much faster than nuclear motion, the internal rotational and vibrational state of the cation is strongly preserved in the neutral intermediate [19]. The resulting fast neutral may be formed in a number of electronically excited Rydberg states of H_3 with geometries similar to H_3^+. In this Letter, we describe an experiment that used translational spectroscopy to study the dynamics of transient H_3 formed by CE of fast H_3^+ with Cs. Fragments that arose from the dissociation of a single H_3 molecule were detected in coincidence using a multiparticle detector, yielding fragment recoil energies and angular correlations. The experimental apparatus, a modified version of an existing spectrometer [20,21], is briefly reviewed here.

An H_3^+ cation beam was generated from a discharge on a pulsed (1 kHz) supersonic expansion of pure H_2 or a 10:1 Ar : H_2 mixture. Experiments on the dissociative charge exchange (DCE) of O_2^+ have shown the resulting beam to be vibrationally cold ($T_{vib} < 300$ K), with rotational temperatures expected to be on the order of 30 K. The cations were skimmed, accelerated to 12 keV, and rereferenced to ground potential by a high-voltage switch. The cation of interest was mass-selected by time-of-flight and electrostatically guided through a $\sim 10^{-5}$ torr Cs vapor cell with a path length of ~ 1 mm and a total interaction volume of ~ 1 mm^3.

After formation of a metastable neutral by charge transfer of H_3^+ with Cs, dissociation occurred via both two- and three-body pathways. DCE products recoiled out of the ion beam axis over a 1 m flight length and impinged on a time- and position-sensitive multiparticle detector [20]. The neutral detector consisted of a set of 4 cm diameter microchannel plates in front of four separate delay-line anodes. Each quadrant allowed detection of up to two fragments per dissociation event, thereby allowing up to eight particles to be measured in coincidence. The position and time-of-arrival were measured for each fragment, allowing a complete three-dimensional kinematic characterization of each dissociation event. Given the parent mass, cation beam energy, and fragment mass ratio, momentum conservation was checked, and the center-of-mass (c.m.) translational energy and product recoil angles were calculated for each event. The neutral detector was calibrated with the well-known 1 and 3 eV features from DCE of O_2^+ with Cs [22].

The three-body c.m. kinetic energy release (KER) spectra for H_3 and D_3 are shown in Fig. 2. Well-resolved features associated with the three-body dissociation of the low-lying metastable Rydberg states to three ground-state atoms are observed. Unresolved features at high KER, formed via NRCE, are observed for the manifolds of $n = 3$ and $n \geq 4$ states (see Fig. 2). The feature at ~ 1.5 eV in H_3 arises from vibrational excitation of the $n = 2$ Rydberg states, presumably due to vibrational excitation in the parent cation beam. Comparison of the KER spectra shows that, as expected, NRCE plays a larger role for H_3 due to the higher relative velocity. For both systems no broad feature associated with direct CE to the repulsive $2p\ ^2E'$ state is observed. It should also be noted that the data assigned to the $2p\ ^2A_2''$ state of H_3 must arise from rotational excitation since the lowest rotational level is long-lived [2].

The Dalitz [23] plot representations for the low-lying Rydberg states in the H_3 and D_3 KER spectra are shown in Fig. 3. The Dalitz plot is constructed by plotting the fractional square of the individual fragment momenta as the distances from the sides of an equilateral triangle. The triangle represents energy conservation and the inscribed circle represents momentum conservation for equal mass fragments. The three-body channel results in three atomic fragments, indistinguishable from one another, yielding a Dalitz plot with six-fold degeneracy and three-fold symmetry. The Dalitz plot allows one to visualize the c.m. momentum partitioning of the fragments in the dissociation [15] (see Fig. 4). Figure 3(f) shows the results of a Monte Carlo simulation of the geometric detector collection efficiency at KER = 2.7 eV (KER of the H_3 $3p\ ^2E'$ state). The collection efficiency for a KER of 1 eV, not shown, is nearly unity for all geometries of H_3 or D_3.

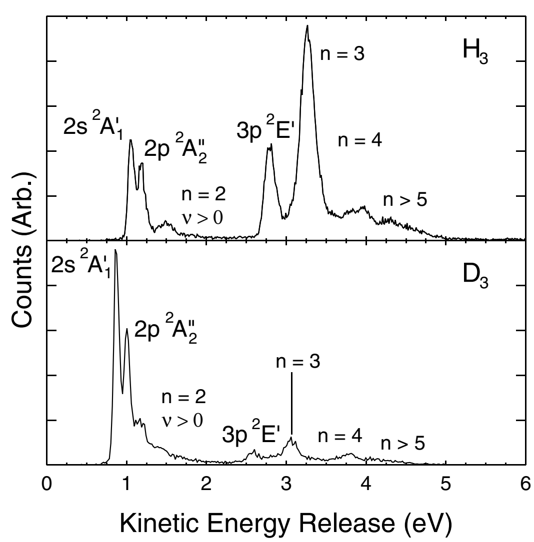

FIG. 2. The center-of-mass kinetic energy release distribution from the three-body dissociation of metastable H_3^* and D_3^* at 12 keV (labels are state assignments).

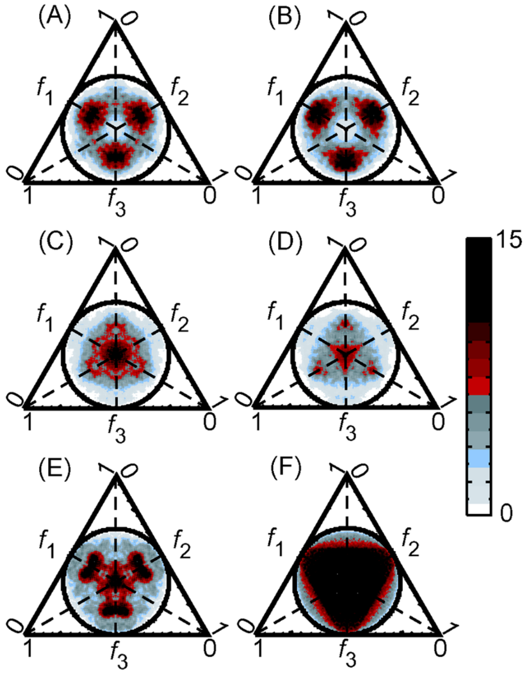

FIG. 3 (color online). Dalitz plot representations for (a,b) the $2s\ ^2A_1'$ state in H_3 and D_3, (c,d) the $2p\ ^2A_2''$ state in H_3 and D_3, (e) the $3p\ ^2E'$ state in H_3, and (f) a Monte Carlo simulation of the detection efficiency at KER $= 2.7$ eV. The axis labels f_i are the fractional square of momentum partitioning ($f_i = p_i^2/\Sigma p_i^2$). The scale is linear from 0 to 15, normalized to the most intense features in each plot.

Correcting the raw data with numerically generated collection efficiencies results in no significant differences, thus the data presented in Fig. 3 is raw data.

Kokoouline and Greene have noted that the normal modes of H_3 (Fig. 1), denoted by the symmetric-stretch Q_1 and degenerate asymmetric stretches Q_x and Q_y are closely related to the nuclear configurations implied by the momentum partitioning shown in the Dalitz plot (see Fig. 4) [11]. This correlation should hold for prompt dissociation of triatomic hydrogen near the symmetric D_{3h} configuration with the assumption that significant exit channel interactions among the three H atom products do not occur. Nuclear motion along the $+Q_x$ coordinate distorts the equilateral C_{3v} configuration to a linear configuration while maintaining C_{2v} symmetry, asymptotically leading to two particles with large momentum and one with nearzero momentum. The $-Q_x$ coordinate corresponds to a C_{2v} distortion correlating with perpendicular insertion of H into and H_2 bond, as shown by the kinematic model of three-body dissociation presented by Maul and Gericke [24]. Motion along the $\pm Q_y$ coordinate correlates with asymmetric momentum partitioning along the bisector of the angle made by the $\pm Q_x$ axes, while motion along Q_1, the symmetric vibration, will lead to equal momentum partitioning and be observed as a feature at the center.

The Dalitz plots corresponding to predissociation of the $2s\ ^2A_1'$ state of H_3 and D_3 are shown in Figs. 3(a) and 3(b). Both systems exhibit a high-density feature shifted off-center along the $+Q_x$ axis indicating that only a restricted range of momentum partitioning and, thus, nuclear configurations undergo facile crossing to the repulsive surface. This observation implies the $2s\ ^2A_1'$ and upper sheet of the dissociative $2p\ ^2E'$ states couple when the nuclei are distorted towards linear geometry. The position of the peaks indicate that the nominal angles between the c.m. momentum vectors of the atomic products are $(\alpha, \beta, \gamma) \approx (144°, 108°, 108°)$ and $(148°, 106°, 106°)$, as defined in Fig. 1, for H_3 and D_3, respectively. The coupling of the $2s\ ^2A_1'$and $2p\ ^2E'$ states must occur via vibronic interactions of the degenerate (Q_x and Q_y) vibrations of e' symmetry [25]. The data presented here only arise from dissociation of the ground vibrational state of $2s\ ^2A_1'$ H_3 and D_3; therefore, the coupling to the $2p\ ^2E'$ state occurs via zero-point vibrational motion along the $+Q_x$ coordinate. Within the Born-Oppenheimer approximation the PESs are identical for H_3 and D_3; thus, the subtle isotope effect must arise from the smaller amplitude zero-point wave function for D_3.

The Dalitz plots for events corresponding to predissociation of the $2p\ ^2A_2''$ state of H_3 and D_3 are shown in Figs. 3(c) and 3(d). Both systems exhibit a high-density feature at the center and features along the symmetry axes spreading into the asymmetric region. The center feature indicates that dissociation is most favorable near the symmetric C_{3v} configuration, corresponding to nuclear motion along the Q_1 coordinate. This observation is

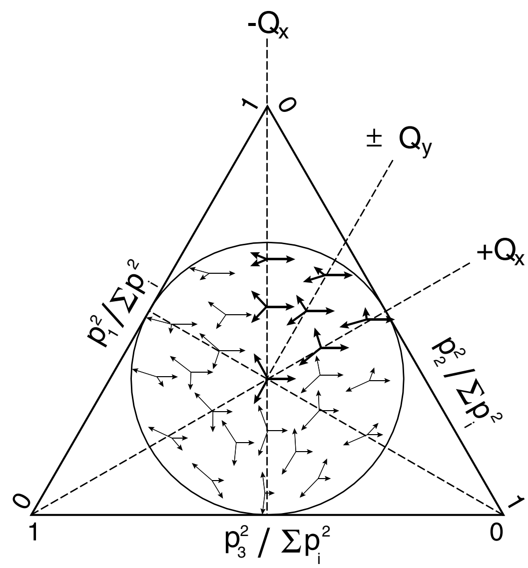

FIG. 4. The Dalitz plot represented as a map of the momentum partitioning among the three atomic fragments. The correlation with the asymmetric normal vibrations of H_3 is highlighted in one-sixth of the plot.

reasonable since the $2p\ ^2A_2''$ state couples to the $2p\ ^2E'$ state via rotation [26] and is not expected to appreciably distort the initial C_{3v} nuclear configuration. The weaker off-center features are not as prominent and show an isotope effect. H_3 exhibits a weak feature along both the $\pm Q_x$ axes corresponding to product c.m. momentum vectors having $(\alpha, \beta, \gamma) \approx (140°, 110°, 110°)$ along $-Q_x$ and $(137°, 137°, 86°)$ along $+Q_x$. The dissociation of D_3 with a $\pm Q_x$ nuclear distortion is markedly different. The D_3 data shows a feature corresponding to a $-Q_x$ distortion with the same $(\alpha, \beta, \gamma) \approx (137°, 137°, 86°)$ as H_3. However, it is broader and more pronounced for D_3. In addition, a weak feature is observed along the $+Q_x$ axis with $(\alpha, \beta, \gamma) \approx (160°, 100°, 100°)$. No feature corresponding to a near-linear distortion of this magnitude is observed for H_3.

The Dalitz plot for events corresponding to the predissociation of the $3p\ ^2E'$ state of H_3 is shown in Fig. 3(e). While this state is also resolved for D_3, insufficient data was obtained to generate a useful Dalitz plot. High-density features are observed in both the central symmetric region and slightly off the $+Q_x$ axis. Kokoouline and Greene have calculated the PES for the doubly degenerate $3p\ ^2E'$ state and resulting Jahn-Teller surfaces [11]. The lower surface has three minima, two have configurations involving $(-Q_x \pm Q_y)$ motion, and one is along the $+Q_x$ axis. The asymmetric feature in the Dalitz plot is consistent with the calculated minimum on the $+Q_x$ axis except for the low density measured directly on the axis. More specifically, the peak asymmetric feature corresponds to c.m. product momentum vectors with $(\alpha, \beta, \gamma) \approx (146°, 116°, 98°)$. The physical mechanism responsible for this Dalitz plot is not clear; however, it is known that immediately after CE to the $3p\ ^2E'$ state the nuclear configuration has C_{3v} symmetry and begins to undergo a Jahn-Teller distortion toward the lower sheet minima. It is possible that the high-density regions of the momentum partitioning observed in the Dalitz plot trace the prompt evolution of the nuclei as three-body predissociation occurs along the path to the distorted minimum along the $+Q_x$ axis.

The Dalitz plot shown in Fig. 3(e) is consistent with the recently reported results of Galster *et al.* for the dissociation of $3p\ ^2E'$ H_3 [17]. In that study, the $3p\ ^2E'$ state H_3 was formed by rapid spontaneous emission of the $3d\ ^2E''$ state prepared by laser excitation of the long-lived $2p\ ^2A_2''$ state. The agreement between these two studies is notable as distinct methods of preparation and detection have been used, providing the first experimental confirmation of the three-body dynamics of this fundamental system. In addition, the results of these studies show that three-body predissociation is competitive with radiative decay processes.

In conclusion, these experiments reveal the state-specific three-body dissociation dynamics for the lowest metastable Rydberg states of H_3 and D_3. A considerable isotope effect on the three-body dissociation dynamics is observed, particularly fort the $2p\ ^2A_2''$ state. These results provide valuable empirical information and an impetus for more rigorous theoretical investigations of the nonadiabatic couplings and dynamics that govern the three-body dissociation of H_3 and D_3. Quantum wave packet dynamics calculations on the coupled excited-state PESs for this fundamental system will be of considerable value for further interpretations of the present results.

This work was supported by the U.S. Air Force Office of Scientific Research under Grants No. F49620-03-1-0039 and No. FA9550-04-1-0035. We thank Dr. Morton A. Fineman for his contributions to this research.

*Electronic address: rcontinetti@ucsd.edu

[1] H. Figger *et al.*, Can. J. Phys. **62**, 1274 (1984).
[2] C. Bordas, P. C. Cosby, and H. Helm, J. Chem. Phys. **93**, 6303 (1990).
[3] W. D. Watson, Astrophys. J. **183**, L17 (1973).
[4] B. J. McCall *et al.*, Astrophys. J. **522**, 338 (1999).
[5] T. Oka, in *Dissociative Recombination of Molecular Ions with Electrons*, edited by S. Guberman (Kluwer, Plenum, New York, 2003), p. 209.
[6] M. Larsson, Philos. Trans. R. Soc. London A **358**, 2433 (2000).
[7] D. Strasser *et al.*, Phys. Rev. A **66**, 032719 (2002).
[8] B. J. McCall *et al.*, Nature (London) **422**, 500 (2003).
[9] V. Kokoouline, C. H. Greene, and B. D. Esry, Nature (London) **412**, 891 (2001).
[10] V. Kokoouline and C. H. Greene, Phys. Rev. Lett. **90**, 133201 (2003).
[11] V. Kokoouline and C. H. Greene, Phys. Rev. A **68**, 012703 (2003).
[12] I. D. Petsalakis, G. Theodorakopoulos, and J. S. Wright, J. Chem. Phys. **89**, 6850 (1988).
[13] D. Strasser *et al.*, Phys. Rev. A **65**, 010702 (2001).
[14] U. Müller and P. C. Cosby, Phys. Rev. A **59**, 3632 (1999).
[15] U. Müller *et al.*, Phys. Rev. Lett. **83**, 2718 (1999).
[16] U. Galster *et al.*, Eur. Phys. J. D **17**, 307 (2001).
[17] U. Galster, U. Müller, and H. Helm, Phys. Rev. Lett. **92**, 073002 (2004).
[18] V. Sidis and D. P. de Bruijn, Chem. Phys. **85**, 201 (1984).
[19] M. R. Spalburg, J. Los, and E. A. Gislason, Chem. Phys. **94**, 327 (1985).
[20] K. A. Hanold *et al.*, Rev. Sci. Instrum. **70**, 2268 (1999).
[21] T. G. Clements and R. E. Continetti, Phys. Rev. Lett. **89**, 033005 (2002).
[22] W. J. van der Zande *et al.*, Chem. Phys. Lett. **140**, 175 (1987).
[23] R. H. Dalitz, Philos. Mag. **44**, 1068 (1953).
[24] C. Maul and K.-H. Gericke, J. Phys. Chem. A **104**, 2531 (2000).
[25] I. Dabrowski and G. Herzberg, Can. J. Phys. **58**, 1238 (1980).
[26] G. Herzberg, J. T. Hougen, and J. K. G. Watson, Can. J. Phys. **60**, 1261 (1982).